

# The KMTNet/K2-C9 (*Kepler*) Data Release

H.-W. KIM<sup>1</sup>, K.-H. HWANG<sup>1</sup>, D.-J. KIM<sup>1</sup>, M. D. ALBROW<sup>2</sup>, S.-M. CHA<sup>1,3</sup>, S.-J. CHUNG<sup>1,4</sup>, A. GOULD<sup>1,5,6</sup>, C. HAN<sup>7</sup>, Y. K. JUNG<sup>8</sup>, S.-L. KIM<sup>1,4</sup>, C.-U. LEE<sup>1,4</sup>, D.-J. LEE<sup>1</sup>, Y. LEE<sup>1,3</sup>, B.-G. PARK<sup>1,4</sup>, R. W. POGGE<sup>5</sup>, Y.-H. RYU<sup>1</sup>, I.-G. SHIN<sup>8</sup>, Y. SHVARTZVALD<sup>9,†</sup>, J. C. YEE<sup>8</sup>, W. ZANG<sup>10,11</sup>, W. ZHU<sup>12</sup>,  
(KMTNET COLLABORATION)

<sup>1</sup>*Korea Astronomy and Space Science Institute, Daejeon 34055, Korea*

<sup>2</sup>*University of Canterbury, Department of Physics and Astronomy, Private Bag 4800, Christchurch 8020, New Zealand*

<sup>3</sup>*School of Space Research, Kyung Hee University, Yongin, Gyeonggi 17104, Korea*

<sup>4</sup>*Astronomy and Space Science Major, Korea University of Science and Technology, Daejeon 34113, Korea*

<sup>5</sup>*Department of Astronomy, Ohio State University, 140 W. 18th Ave., Columbus, OH 43210, USA*

<sup>6</sup>*Max-Planck-Institute for Astronomy, Königstuhl 17, 69117 Heidelberg, Germany*

<sup>7</sup>*Department of Physics, Chungbuk National University, Cheongju 28644, Republic of Korea*

<sup>8</sup>*Harvard-Smithsonian CfA, 60 Garden St., Cambridge, MA 02138, USA*

<sup>9</sup>*Jet Propulsion Laboratory, California Institute of Technology, 4800 Oak Grove Drive, Pasadena, CA 91109, USA*

<sup>10</sup>*Physics Department and Tsinghua Centre for Astrophysics, Tsinghua University, Beijing 100084, China*

<sup>11</sup>*Department of Physics, Zhejiang University, Hangzhou, 310058, China*

<sup>12</sup>*Canadian Institute for Theoretical Astrophysics, University of Toronto, 60 St George Street, Toronto, ON M5S 3H8, Canada*

<sup>†</sup>*NASA Postdoctoral Program Fellow*

**ABSTRACT**

We present Korea Microlensing Telescope Network (KMTNet) light curves for microlensing-event candidates in the *Kepler* K2 C9 field having peaks within 3 effective timescales of the *Kepler* observations. These include 181 “clear microlensing” and 84 “possible microlensing” events found by the KMTNet event finder, plus 56 other events found by OGLE and/or MOA that were not found by KMTNet. All data for the first two classes are immediately available for public use without restriction.

*Subject headings:* gravitational lensing; micro

## 1. Introduction

After *Kepler* lost its second reaction wheel, Gould & Horne (2013) proposed that it should become a “microlens parallax satellite”, a concept first advanced by Refsdal (1966) a half-century earlier and further articulated by Gould (1994). By observing the same event simultaneously from two platforms separated by of order 1 AU, one can measure the projected velocity, basically the ratio of the lens-source relative proper motion,  $\boldsymbol{\mu}_{\text{rel}}$ , to their relative parallax,  $\pi_{\text{rel}}$ ,

$$\tilde{\mathbf{v}} \equiv \text{AU} \frac{\boldsymbol{\mu}_{\text{rel}}}{\pi_{\text{rel}}}. \quad (1)$$

By itself, this quantity is a powerful constraint on the otherwise poorly determined lens properties (Han & Gould 1995; Calchi Novati et al. 2015; Zhu et al. 2017a). Moreover, if the Einstein radius  $\theta_{\text{E}}$  is also measured (as is often the case for binary and planetary events), then the projected velocity  $\tilde{\mathbf{v}}$ , or equivalently the microlens parallax,

$$\boldsymbol{\pi}_{\text{E}} \equiv \frac{\pi_{\text{rel}} \boldsymbol{\mu}_{\text{rel}}}{\theta_{\text{E}} \mu_{\text{rel}}}, = \frac{\text{AU} \tilde{\mathbf{v}}}{t_{\text{E}} \tilde{v}^2}, \quad (2)$$

enables measurements of both  $\pi_{\text{rel}} = \theta_{\text{E}} \pi_{\text{E}}$  and the lens mass  $M = (4c^2/G) \tilde{v} t_{\text{E}} \theta_{\text{E}}$  (Gould 1992). Here  $t_{\text{E}} = \theta_{\text{E}} / \mu_{\text{rel}}$  is the Einstein timescale.

Up until the time of the proposal by Gould & Horne (2013), there had been only one successful microlens parallax measurement, which had been carried out by *Spitzer* toward the Small Magellanic Cloud (Dong et al. 2007). Eventually *Spitzer* would observe many hundreds of microlensing events (Gould et al. 2013, 2014, 2015a,b, 2016). However, the point that we wish to emphasize here is the fundamental difference between *Spitzer* and *Kepler* microlensing. With its narrow-angle camera *Spitzer* must point at individual microlensing events, and hence an event must be recognized as interesting before *Spitzer* can start observing it. Moreover, due to operational constraints, *Spitzer* cannot begin observing an event

until 3–9 days after the event is singled out for observations (Figure 1 of Udalski et al. 2015). On the other hand, *Spitzer* has the advantage that it can be pointed at any microlensing event over the  $\sim 100 \text{ deg}^2$  field in which they are discovered.

By contrast, *Kepler* must observe continuously for many weeks without receiving instructions from Earth and so cannot be pointed at any particular event (with the exception of a few extremely long ones). On the other hand, it does observe over a wide enough field that a significant number of stars within this field undergo microlensing events. It therefore observes many microlensing events without specific targeting, and thus independently of the discovery of these events from the ground. Unfortunately, although the full *Kepler* field is  $\sim 100 \text{ deg}^2$ , memory constraints restrict the contiguous area of observations to  $\sim 4 \text{ deg}^2$ . Nevertheless, this area can be chosen to contain some of the densest microlensing fields. See Henderson et al. (2016).

These different engineering characteristics lead to very different regimes of high science performance. In particular, *Kepler* is far better suited to the study of very short timescale events, especially those due to free-floating planets (FFPs) because these are typically over before *Spitzer* could target them. Hence, study of (or constraints upon) FFPs were major goals for the *Kepler* K2 C9 campaign, which operated from April 22.596 to July 2.936 2016.

It was recognized from the beginning, both by NASA and the microlensing community, that the analysis of *Kepler* microlensing data would be exceptionally difficult because the microlensing fields are extremely crowded while *Kepler* has  $4''$  pixels. Moreover, in its two-wheel mode, *Kepler* oscillates on a not-quite-repeating 6-hour cycle. Nevertheless Zhu et al. (2017b) solved many of the photometry problems and applied these solutions to several different events (Zhu et al. 2017b,c; Ryu et al. 2017). However, the Zhu et al. (2017b) approach requires a lot of tender loving care (TLC), and this increases the premium on identifying events that are likely to have scientific importance.

*Kepler* K2 C9 microlensing was strongly supported by several microlensing surveys. The Optical Gravitational Lensing Experiment (Udalski et al. 1994) (OGLE)<sup>1</sup> altered their observing strategy so that the cadence of all five of their fields that strongly overlap the K2 C9 superstamp were observed at OGLE’s maximum rate,  $\Gamma = 3 \text{ hr}^{-1}$ , during the K2 C9 observations. OGLE also identified 54 long timescale events within the K2 C9 field but outside the superstamp, for individual K2 C9 observations. The Microlensing Observations in Astrophysics (Bond et al. 2004) (MOA)<sup>2</sup> collaboration also altered its observing strategy

---

<sup>1</sup><http://ogle.astrouw.edu.pl/ogle4/ews/ews.html>

<sup>2</sup><http://www.massey.ac.nz/~iabond/moa/alert2016/alert.php>

to support K2 C9. Six MOA fields overlap the superstamp, four of which are usually observed at the highest cadence  $\Gamma = 4 \text{ hr}^{-1}$  but one at very low cadence. This field was upgraded to  $\Gamma = 1.2 \text{ hr}^{-1}$ .

In addition, there were several special surveys devoted to the K2 C9 field, The first two of these were both in Hawaii. Using the Canada-France-Hawaii Telescope (CFHT), the 2016 CFHT-K2C9 Multi-color Microlensing Survey (Zang et al. 2018) conducted an independent survey in the  $g$ -,  $r$ -, and  $i$ -bands, which together cover almost the entire *Kepler* bandpass. The CFHT data can be used to predict the magnitude in the Kepler bandpass  $K_p$ , which, has an uncertainty of 0.02 mag in the  $(K_p - r)$  color for typical microlensing events.

The United Kingdom Infrared Telescope (UKIRT) survey (Shvartzvald et al. 2017) observed the entire K2 C9 superstamp in the near infrared. The observations covered 91 nights from April 8 to July 8, with a nominal cadence of 2–3 per night. The data are available at <https://exoplanetarchive.ipac.caltech.edu/docs/UKIRTMission.html> .

The LCOGT Network (Brown et al. 2013) conducted a survey using 1m telescopes equipped with  $26' \times 26'$  cameras at three sites in  $i$ -band. From Australia, they observed 19 fields in the K2 C9 superstamp, while from Chile and South Africa they observed 10 fields containing high magnification events, from both the superstamp and the additional events mentioned above.

The Korea Microlensing Telescope Network (KMTNet, Kim et al. 2016) supported the K2 C9 campaign in three ways. First, we altered our observing strategy to temporarily increase the cadence on the K2 C9 superstamp. This superstamp is covered by two KMTNet fields BLG02 and BLG03 (together with their slightly offset counterparts BLG42 and BLG43). Each KMTNet field is  $4 \text{ deg}^2$ . Under our standard observing protocol for 2016, these two fields were observed at a cadence  $\Gamma = 4 \text{ hr}^{-1}$  from each of our three observatories, in Chile (KMTC), South Africa (KMTS), and Australia (KMTA). However, for all but the final 15 days of K2 C9 (during which *Spitzer* microlensing began), we increased the cadence at KMTS and KMTA to  $\Gamma = 6 \text{ hr}^{-1}$ . That is, the special K2 observing protocol was in force from April 23 to June 16.

Second, we altered our data policy for all events that are independently discovered by KMTNet and that peak in or near the K2 C9 window. KMTNet generally aims to make all of our microlensing light curves publicly available in a timely fashion (Kim et al. 2018). However, as discussed in Section 5, we have further relaxed this policy for KMTNet-discovered K2 C9 events.

Third, for the special case of K2 C9 events, we are also making publicly available all KMTNet data for microlensing events found by other groups (in practice, OGLE and MOA),

but that were not independently identified by KMTNet. In this case, however, we require that prospective users of these data obtain permission from the discovering group(s) before publishing them.

## 2. 2016 Event Finder

The events presented here were found by applying the KMTNet event finder to 2016 data that overlap the K2 C9 field and then excluding those events that peak well outside the K2 C9 window. The KMTNet event finder was described in detail by Kim et al. (2018). In brief, each light curve is fit to a dense grid of point-lens models, parametrized by  $(t_0, t_{\text{eff}}, u_0)$ , where  $t_0$  is the peak time,  $t_{\text{eff}}$  is the effective timescale, and  $u_0$  is the impact parameter. Because the fit is carried out only on the interval  $t_0 \pm 5 t_{\text{eff}}$ , the  $u_0$  sampling can be reduced to just two values (0 and 1), yet still remain “dense” (Kim et al. 2018). Those events that pass a  $\chi^2$  threshold are cataloged. Then these are grouped by a “friends-of-friends” algorithm. The output is shown to an operator in several different displays, who then classifies them as “clear microlensing”, “possible microlensing”, or as one of several classes of variables or artifacts.

Here, we describe in greater detail only the changes in the 2016 version of the algorithm relative to 2015. The most important change is that data from all three observatories are fitted simultaneously to the same model. (In 2015, by contrast, only the KMTC data were fitted. Then, only if the event passed the  $\chi^2$  threshold and was subsequently selected by the operator, would the KMTS and KMTA data be reduced and inspected.)

Second, for the cases that the same star is observed in two or more KMTNet fields, we fit all the light curves simultaneously when possible. This was not necessary for 2015 because there were no overlapping fields. In 2016, however, fields (BLG01, BLG02, BLG03) were observed slightly offset as (BLG41, BLG42, BLG43). See Figure 12 of Kim et al. (2018). In addition, BLG02 and BLG03 have a quite significant overlap (roughly  $0.4 \text{ deg}^2$ ), which lies almost entirely in the K2 C9 superstamp. Thus, there can be up to four overlapping fields, in which case we would fit 12 light curves simultaneously. (In fact, there are very occasionally five overlapping fields). However, we are able to unambiguously identify two catalog stars from different fields as being the “same star” only for regions covered by the OGLE-III star catalog (Szymański et al. 2011). That is, for these regions, our input catalog is derived from OGLE-III, and so is identical for all fields. However, for regions not covered by OGLE-III, for which our star catalog is derived from DoPhot (Schechter et al. 1993) analysis of KMTNet images, we must analyze the light curves from different fields independently (although the light curves from different observatories are still analyzed jointly).

Third, we set a  $\chi^2 > 500$  threshold for all stars that lie in one of the six fields, BLG01, BLG02, BLG03, BLG41, BLG42, BLG43, and that lack OGLE-III counterparts. For the remaining stars (roughly 95% of the total), i.e., those lying in these six fields that have OGLE-III counterparts as well as all stars that lie in other fields, we adopt  $\chi^2 > 1000$ .

The reason for using two different  $\chi^2$  thresholds is that light curves in the first category have potentially confirming information from other fields, while those in the second do not.

Fourth, while Kim et al. (2018) expressed the hope that the event finder could be applied to very short effective timescales in 2016, in fact this proved impractical due to an excess of spurious candidate events. Hence, we adopt  $t_{\text{eff}} \geq 1$  day. This is a significant shortcoming, particularly for the K2 C9 field, for which FFPs are especially important. We are currently working on an alternate algorithm for very short events. If successful, we will also release the data for those events. However, we do not wish to delay the present release.

Fifth, we cross-checked all candidates against variables and artifacts that were identified in 2015 as well as against all published variables that we could identify. However, because the field locations (and so star catalogs) changed between 2015 and 2016, we could cross-check against 2015 only for OGLE-III catalog stars.

Sixth, for each event we inspected the combined 2016+2017 light curve, thereby removing 49 variables, mostly cataclysmic variables (CVs), but also other episodic repeaters as well as a few long-period variables.

Finally, we note that several improvements were made during the 2016 analysis. These all occurred after the K2 C9 superstamp was processed and so apply only to other fields, but we briefly mention them here. A complete description will be given in the 2016 season data release paper. First, we created a new periodic-variable finder, which was applied to the candidates (after being grouped). Second we created an algorithm to identify an important class of short-timescale artifacts, which was also applied to grouped candidates in 2016 but which is being incorporated directly into the event finder for 2017 and future years.

### 3. K2 C9 Selection

Light curves are identified for publication within this K2 C9 release provided that they meet two criteria. First, they must lie in the K2 C9 field as determined by the `K2fov` algorithm, which is available at <https://keplerscience.arc.nasa.gov/software.html>. This includes both events in the superstamp and any of the 37 (out of 54) “postage stamps” that overlap

the KMTNet fields. Second,  $t_0$  must lie in the range,

$$t_{\text{K2C9,-}} - 3t_{\text{eff}} < t_0 < t_{\text{K2C9,+}} + 3t_{\text{eff}}, \quad (3)$$

where  $t_0$  and  $t_{\text{eff}}$  are the best-fit values as determined by the event finder and  $t_{\text{K2C9},\pm}$  are the start and end times of the K2 C9 campaign.

Our supplementary release of KMTNet data for events found by other groups is defined as follows. First, it is restricted to events that were not found by the KMTNet event finder for 2016 as a whole. Second, the event must lie in the K2 C9 field as determined by the K2fov algorithm. Third, it must satisfy Equation (3) but with  $t_0$  and  $t_{\text{eff}}$  derived from the fit announced by OGLE (if OGLE found it) or, if not, by the discovery group. The value of  $t_0$  is simply the one that is reported, while  $t_{\text{eff}} \equiv \min(u_0, 1)t_{\text{E}}$ , where  $u_0$  and  $t_{\text{E}}$  are the reported impact parameter and Einstein timescale, respectively.

These prescriptions should include the overwhelming majority of events that have useful *Kepler* data. However, if there are others (and if reasonable scientific justification is given), we will provide data for these upon request.

Figure 1 shows the sky positions of the events with data that are being released. The red and blue points indicate “clear” and “possible” microlensing events found by the KMTNet event finder, respectively. The gold points are events found by OGLE but not by KMTNet. The purple points are events found by MOA only.

#### 4. Data Products

The data are available at the website <http://kmtnet.kasi.re.kr/ulens/> with subpages for this paper at <http://kmtnet.kasi.re.kr/ulens/event/2016k2/> and <http://kmtnet.kasi.re.kr/ulens/event/2016nonkmt/>. For each event that was found independently by KMTNet (181 “clear”, 84 “possible”), there are two reductions. The first is the difference imaging analysis (DIA) used to identify the events, which is derived from publicly available Woźniak (2000) code. The second is a pySIS reduction employing the code of Albrow et al. (2009). In most cases, the latter is substantially better, but it can fail completely in some cases. These can easily be identified by the pictorial representations on the webpage. We note that it may in principle be possible to recover from these failures using a TLC approach, but we do not generically attempt to do so and such TLC light curves are not part of this release.

The pages also contain diagnostic information similar to that of Kim et al. (2018), i.e., finding charts, diagnostic images, parameters from the fit, as well as the identifier names of

events found by other surveys.

For the 56 events that were not independently found by KMTNet, the pages contain pySIS reductions but not DIA reductions.

## 5. Data Policy

For K2 C9 events found by KMTNet, there is no restriction whatever on the use of the released light curves, other than to cite this paper. For K2 C9 events found by other groups, but not found by KMTNet, use of the KMTNet data requires consent of the discovery group(s).

Work by WZ, YKJ, and AG were supported by AST-1516842 from the US NSF. WZ, IGS, and AG were supported by JPL grant 1500811. This research has made use of the KMTNet system operated by the Korea Astronomy and Space Science Institute (KASI) and the data were obtained at three host sites of CTIO in Chile, SAAO in South Africa, and SSO in Australia. Work by C.H. was supported by the grant (2017R1A4A101517) of National Research Foundation of Korea. Work by YS was supported by an appointment to the NASA Postdoctoral Program at the Jet Propulsion Laboratory, California Institute of Technology, administered by Universities Space Research Association through a contract with NASA.

## REFERENCES

- Albrow, M. D., Horne, K., Bramich, D. M., et al. 2009, MNRAS, 397, 2099
- Bond, I.A., Udalski, A., Jaroszyński, M. et al. 2004, ApJ, 606, L155
- Brown, T.M., Baliber, N., Bianco, F.B. et al. 2013, PASP, 125, 1031
- Calchi Novati, S., Gould, A., Udalski, A., et al., 2015, ApJ, 804, 20
- Dong, S., Udalski, A., et al. 2007, ApJ, 664, 862
- Gould, A. 1992, ApJ, 392, 442
- Gould, A. 1994, ApJ, 421, L75
- Gould, A. & Horne, K. 2013, ApJ, 779, L28
- Gould, A., Carey, S., & Yee, J. 2013, spitz.prop 10036



- Gould, A., Carey, S., & Yee, J. 2014 spitz.prop 11006
- Gould, A., Yee, J., & Carey, S. 2015a spitz.prop 12013
- Gould, A., Yee, J., & Carey, S. 2015b spitz.prop 12015
- Gould, A., Carey, S., & Yee 2016 spitz.prop 13005
- Han, C. & Gould, A. 1995, ApJ, 447, 53
- Henderson, C.B., Poleski, R., Penny, M. et al. 2016 PASP128, 124401
- Kim, D.-J., Kim, H.-W., Hwang, K.-H., et al., 2018, AJ, in press
- Kim, S.-L., Lee, C.-U., Park, B.-G., et al. 2016, JKAS, 49, 37
- Refsdal, S. 1966, MNRAS, 134, 315
- Ryu, Y.H, Yee, J.C., Udalski, A. et al. 2017, AJ, in press
- Schechter, P.L., Mateo, M., & Saha, A. 1993, PASP, 105, 1342
- Shvartzvald, Y., Bryden, G., Gould, A. et al. 2017, AJ, 153,61
- Szymański, M.K., Udalski, A., Soszyński, I., et al. 2011, Acta Astron., 61, 83
- Udalski, A., Szymanski, M., Kaluzny, J., Kubiak, M., Mateo, M., Krzeminski, W., & Paczyński, B. 1994, Acta Astron., 44, 227
- Udalski, A., Yee, J.C., Gould, A., et al. 2015, ApJ, 799, 237
- Woźniak, P. R. 2000, Acta Astron., 50, 421
- Zang, W., Penny, M., Zhu, W. 2018, in prep
- Zhu, W., Udalski, A., Calchi Novati, S., et al. 2017a, ApJ, in press, arXiv:1701.05191
- Zhu, W., Huang, C., Udalski, A., et al. 2017b, PASP, 129, 104501
- Zhu, W., Udalski, A., Huang, C., et al. 2017b, ApJ, in press, arXiv:1709.09959

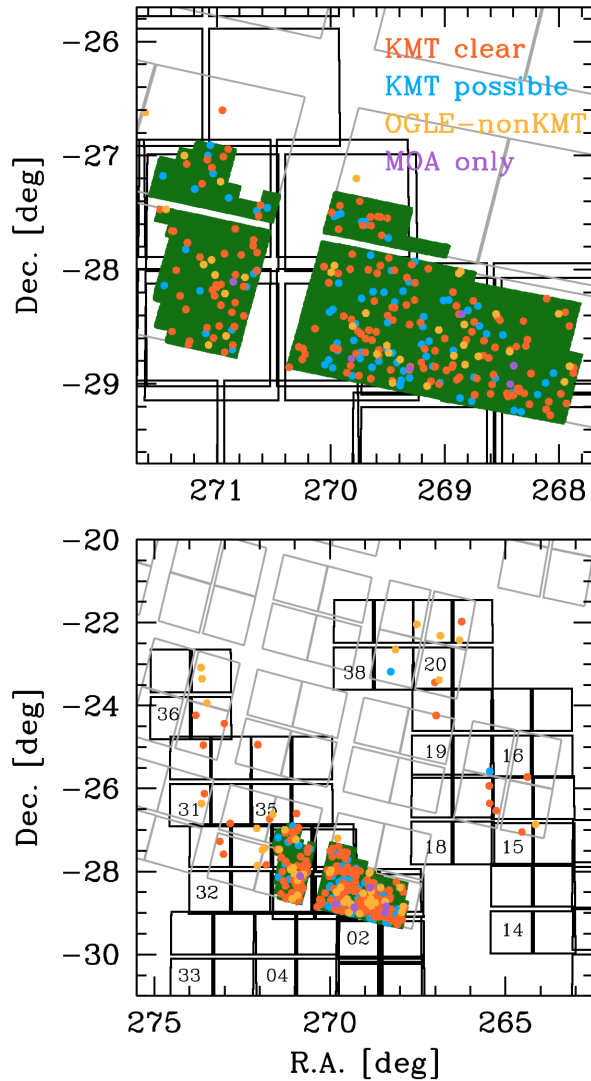


Fig. 1.— Microlensing events with KMTNet data in the *Kepler* K2 C9 field. The main superstamp is shown in green. Events that were independently identified as “clear” or “possible” microlensing are shown in red and blue, respectively. Events found by OGLE but not KMTNet are shown in gold. Those found only by MOA are shown in purple. The active chips of the *Kepler* camera are shown in gray outline, while the KMTNet fields are shown in black outline. When there is sufficient space, the KMTNet field number is given in the lower-left chip. See Figure 12 of Kim et al. (2018) for a more complete representation of these fields.